NUMERICAL DETERMINATION OF LISSAJOUS TRAJECTORIES IN THE RESTRICTED THREE-BODY PROBLEM

K. C. HOWELL and H. J. PERNICKA

School of Aeronautics and Astronautics, Purdue University, West Lafayette, Indiana 47907, *U.S.A.*

(Received: June 25, 1986; in final form: July 16, 1987)

Abstract. In previous studies, Lissajous trajectories associated with the collinear libration points in the restricted three-body problem have been successfully computed analytically to at least third-order. Those approximations are utilized to determine such trajectories numerically for an arbitrary, predetermined number of revolutions in the rotating frame, for the case of circular primary motion. The numerical approach first identifies target positions at specified intervals along the trajectory and locates a continuous path through those points with velocity discontinuities. Then the $\Delta\bar{v}$'s are simultaneously reduced in an iterative process. Such trajectories have been constructed in various primary systems, for a wide range of orbit sizes and a large number of revolutions.

1. Introduction

In the restricted three-body problem a particular type of bounded, three-dimensional solution has been recently studied by a number of authors. These trajectories are generally quasi-periodic and associated with each of the collinear libration points. Farquhar and Kamel [1] used the method of Linstedt–Poincaré to produce a third-order analytic solution for such orbits near the translunar libration point (L_2) in the Earth–Moon system. Richardson and Cary [2] also developed a series solution truncated to fourth order. The Lindstedt method has also been used successfully to investigate three-dimensional orbits in other dynamical systems [3]. These analytic approaches show that the linearized motion near any collinear point includes a periodic path in the plane of primary motion, and an uncoupled periodic out-of-plane motion. The two frequencies are generally unequal. For small amplitudes, the orbital path traces out a Lissajous figure, and thus, the orbits will subsequently be called Lissajous trajectories. When the amplitude is sufficiently large, so that nonlinear terms are significant, certain combinations of in-plane and out-of-plane amplitudes exist such that the corresponding frequencies are equal and a perfectly periodic three-dimensional motion results. Members of this subset of general Lissajous trajectories are sometimes called halo orbits.

Halo orbits have been computed analytically using the series solutions mentioned above [4]. In addition, they have been calculated numerically from the exact nonlinear equations of motion using differential corrections schemes, the results of which appear in references [5] through [8] among others. Lissajous trajectories have been computed analytically from the series solutions but numeric calculation has been limited because of their nonperiodicity. The objective of this work was to produce a continuous, bounded, 'Lissajous' solution numerically from the nonlinear differential equations. The original motivation for this study was actually to

Celestial Mechanics **41** (1988) 107–124.
© 1988 *by Kluwer Academic Publishers.*

determine a nominal Lissajous trajectory to be associated with the interior collinear libration point (L_1) in the Sun–Earth system. Therefore, the constants corresponding to that problem were used primarily. The results, however, are easily generalized to other systems.

In this initial effort, it was assumed that the primaries move in circular orbits. Also, in development of a technique to meet the objective, certain abilities of the resulting method were defined as desirable. Lissajous trajectories exhibit a far greater variety of orbit sizes than halo orbits. The numeric approach should accommodate as much of that range as possible. The approach also needed to be able to find a solution for a possibly predetermined but arbitrary number of revolutions in the rotating frame. At the same time, numerical problems inherent with long integration times had to be minimized.

2. Analysis

2.1. EQUATIONS OF MOTION

The equations governing motion in this problem are written in the form associated with the restricted three-body problem. In the usual rotating coordinate system, the x-axis is always directed from the larger toward the smaller primary. The y-axis is 90° from the x-axis in the primary plane of motion. The z-axis completes the right handed system, defining the out-of-plane direction. The associated unit vectors are $\hat{x}$, $\hat{y}$, $\hat{z}$ respectively. The problem is nondimensionalized such that the following quantities are equal to unity: the sum of the masses of the primaries, the mean distance between them, the mean angular velocity of the coordinate frame, and the gravitational constant. The nondimensional smaller primary mass is represented as μ.

Let the vector $\bar{\rho}$ describe the position of the infinitesimal mass from the center of mass of the primaries such that $\bar{\rho}$ has components **x**, **y** and **z**. In the standard formulation of the circular restricted three-body problem, then, the equations of motion can be written

$$\begin{aligned} \ddot{\mathbf{x}} - 2\dot{\mathbf{y}} &= \frac{\partial U}{\partial \mathbf{x}} \\ \ddot{\mathbf{y}} + 2\dot{\mathbf{x}} &= \frac{\partial U}{\partial \mathbf{y}} \\ \ddot{\mathbf{z}} &= \frac{\partial U}{\partial \mathbf{z}}, \end{aligned} \tag{1}$$

where

$$\begin{aligned} U &= (\mathbf{x}^2 + \mathbf{y}^2)/2 + (1-\mu)/d + \mu/r \\ d &= [(\mathbf{x}+\mu)^2 + \mathbf{y}^2 + \mathbf{z}^2]^{1/2} \\ r &= [(\mathbf{x}-1+\mu)^2 + \mathbf{y}^2 + \mathbf{z}^2]^{1/2}. \end{aligned}$$

Dots denote differentiation with respect to nondimensional time. The equations are known to yield Jacobi's constant of integration, C, given by

$$C = 2U - (\dot{\mathbf{x}}^2 + \dot{\mathbf{y}}^2 + \dot{\mathbf{z}}^2). \tag{2}$$

Also needed is the 6×6 transition matrix, $\Phi(t, t_0)$, of partial derivatives, $\partial X(t)/\partial X(t_0)$, where X is defined as a column vector with elements $\mathbf{x}$, $\mathbf{y}$, $\mathbf{z}$, $\dot{\mathbf{x}}$, $\dot{\mathbf{y}}$, $\dot{\mathbf{z}}$. Here $\Phi(t_0, t_0) = I$, the identity matrix and

$$\frac{\mathrm{d}}{\mathrm{d}t}\Phi(t, t_0) = A(t)\Phi(t, t_0), \tag{3}$$

where

$$A(t) = \left[\begin{array}{c|c} 0 & I \\ \hline U_{XX} & 2\Omega \end{array}\right], \qquad \Omega = \begin{bmatrix} 0 & 1 & 0 \\ -1 & 0 & 0 \\ 0 & 0 & 0 \end{bmatrix},$$

and U_{XX} is the symmetric matrix of second partial derivatives of U with respect to $\mathbf{x}$, $\mathbf{y}$, $\mathbf{z}$ evaluated along the orbit.

2.2. APPROXIMATE ANALYTIC SOLUTION

The equations of motion in (1) can be expanded about the collinear libration point of interest. Define position components x, y, z relative to L_i such that

$$\begin{aligned} x &= \mathbf{x} - (1 - \mu + \gamma) \\ y &= \mathbf{y} \\ z &= \mathbf{z} \end{aligned} \tag{4}$$

where γ is the distance between the libration point and smaller primary and γ is positive when referring to L_2, negative for L_1. The linearized form of the differential equations contains constant coefficients and appears as

$$\begin{aligned} \ddot{x} - 2\dot{y} - (1 + 2c)x &= 0 \\ \ddot{y} + 2\dot{x} + (c - 1)y &= 0 \\ \ddot{z} + cz &= 0. \end{aligned} \tag{5}$$

The solution to the equations in (5) for the out-of plane z motion is simple harmonic. The characteristic equation for the in-plane x–y motion has two real and two imaginary roots. If only the nondivergent mode is excited, the solution is bounded and can be written in the form

$$\begin{aligned} x &= -kA_y \cos(\lambda t + \phi) \\ y &= A_y \sin(\lambda t + \phi) \\ z &= A_z \sin(\nu t + \psi). \end{aligned} \tag{6}$$

The linearized solution is then characterized by the two amplitudes A_y and A_z, and

the two phase angles ϕ and ψ. When the frequencies λ and ν are equal, a halo orbit results which repeats with every revolution. The more general case of unequal frequencies yield Lissajous trajectories which do not quite repeat after each revolution.

The higher order approximations utilize Equation (5) as the first term and are written as functions of ϕ, ψ, A_y and A_z. Farquhar and Kamel developed a third-order analytic solution for small amplitude orbits about L_2 in the Earth–Moon system. Their series included corrections due to solar gravity and lunar eccentricity. The original goal in this study was to determine a Lissajous path near L_1 in the Sun–Earth system. Because of the system similarity, the algorithm originally developed by Richardson and Cary is utilized whenever an analytic result is desired. Richardson and Cary actually seek a solution in the lunar-perturbed Sun–Earth system. The primaries in the 'three-body' system are the Sun and Earth/Moon barycenter. The methods of dual time scales and successive approximations are employed to develop a fourth-order expansion including corrections for the eccentricity of the Earth/Moon barycenter path about the Sun, and the Earth–Moon mass ratio. The result is applicable to orbits associated with L_2 or with the interior point L_1. In the recent work, the algorithm in [2] was fairly easily modified to apply to any system of primaries. Development of the higher order terms is given in detail in the reference.

Figure 1 contains three planar projections of a Lissajous trajectory. It is associated with L_1 in the Sun–Earth/Moon barycenter system as computed from the third-order approximation. In the figure the origin is located at L_1. As usual, ϕ, ψ, A_y and A_z are the input required for the analytic results. Since the third-order solution is plotted in the figure, the maximum amplitudes at each revolution will not necessarily coincide with the input values. The input values merely provide a basis for reference in selecting orbit parameters. In Figure 1, the input phase angles $\phi = 180°$ and $\psi = 90°$ are the values used consistently in all the later examples. Those values insure a starting position in the first quadrant of the x–z plane which was chosen for convenience. The input amplitudes are $A_y = A_z = 200\,000$ km, which were also arbitrarily selected for illustration.

2.3. NUMERICAL SOLUTION

2.3.1. *General Approach*

The focus of this work is the determination of a continuous, bounded path as a result of the integration of the exact equations of motion. If the third-order analytic approximation is used to locate initial conditions in a numerical integration, the solution will generally diverge quite rapidly. The method developed provides improved initial conditions as well as required values of all six elements in the state vector at specified intervals along the path, such that integrated trajectories can be 'patched' together for a continuous, bounded motion. In most cases, the intervals are

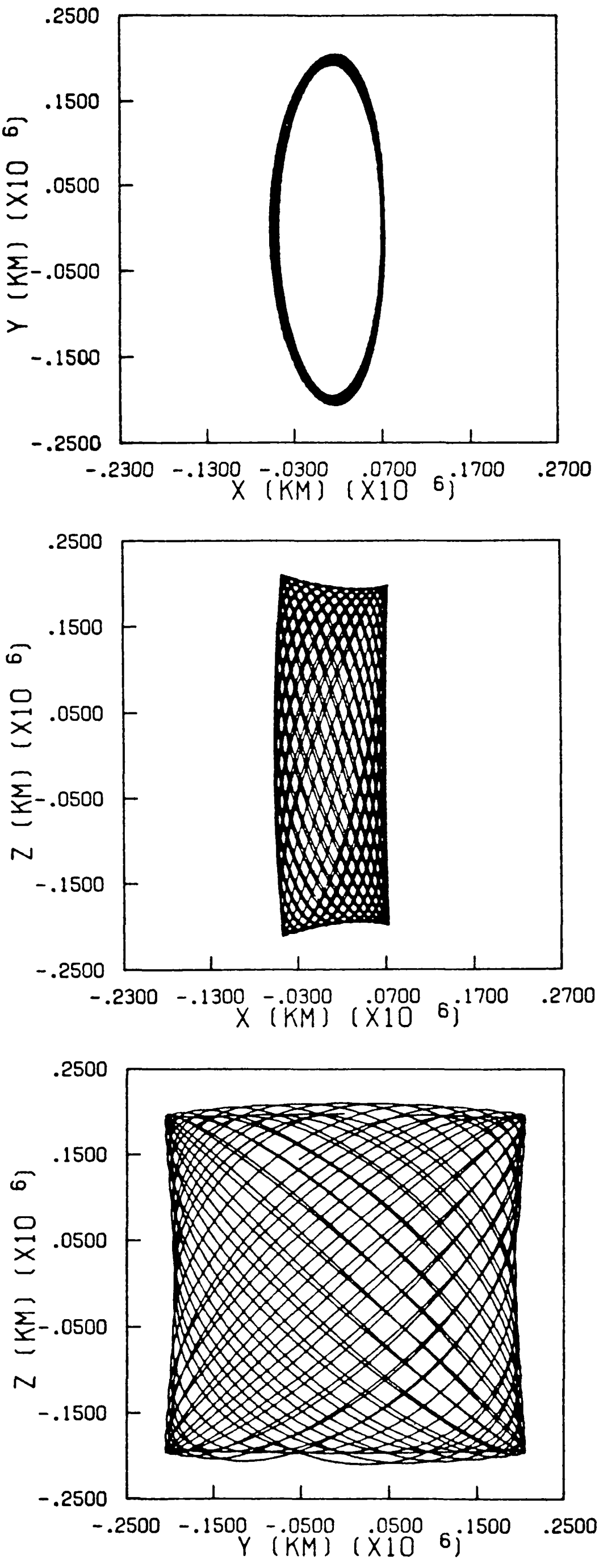

Fig. 1. Third-order L_1 Lissajous solution ($A_y = A_z = 200\,000$ km).

designated as approximately half of a revolution, although use of quarter revolutions was examined as well. The state vectors at the beginning and end of each interval are defined as six-dimensional target points. An integrated path between target points is defined as a trajectory segment.

The procedure is a two level iterative process. Initially all target points are identified. Trajectory segments between target positions are determined by iterating utilizing differential corrections. The segments are patched together such that an orbit results which is continuous in position but that contains a finite number of velocity discontinuities ($\Delta\bar{v}$'s). Then, a linear correction is made to all target positions as well as segment times, with the objective of a simultaneous reduction of the $\Delta\bar{v}$'s. New trajectory segments are determined and patched together at the new target positions resulting in smaller $\Delta\bar{v}$'s. The process continues until the $\Delta\bar{v}$'s are all below some acceptable level, such that the trajectory is essentially continuous in velocity as well as position. Below, a one revolution example is presented first, then the more general equations are discussed.

2.3.2. *Determination of a Path Continuous in Position*

As an example, the method is summarized for the case of a one revolution Lissajous trajectory, i.e. the patching of two trajectory segments. The solid line in Figure 2 represents the two segments. Target point '*o*' is the point of origin of the first segment. Point '*p*' is the endpoint of the first segment and initial point of the second segment. It is also the patch point (or maneuver point) between the segments. The endpoint of segment two is point '*f*', also the final point of the one revolution

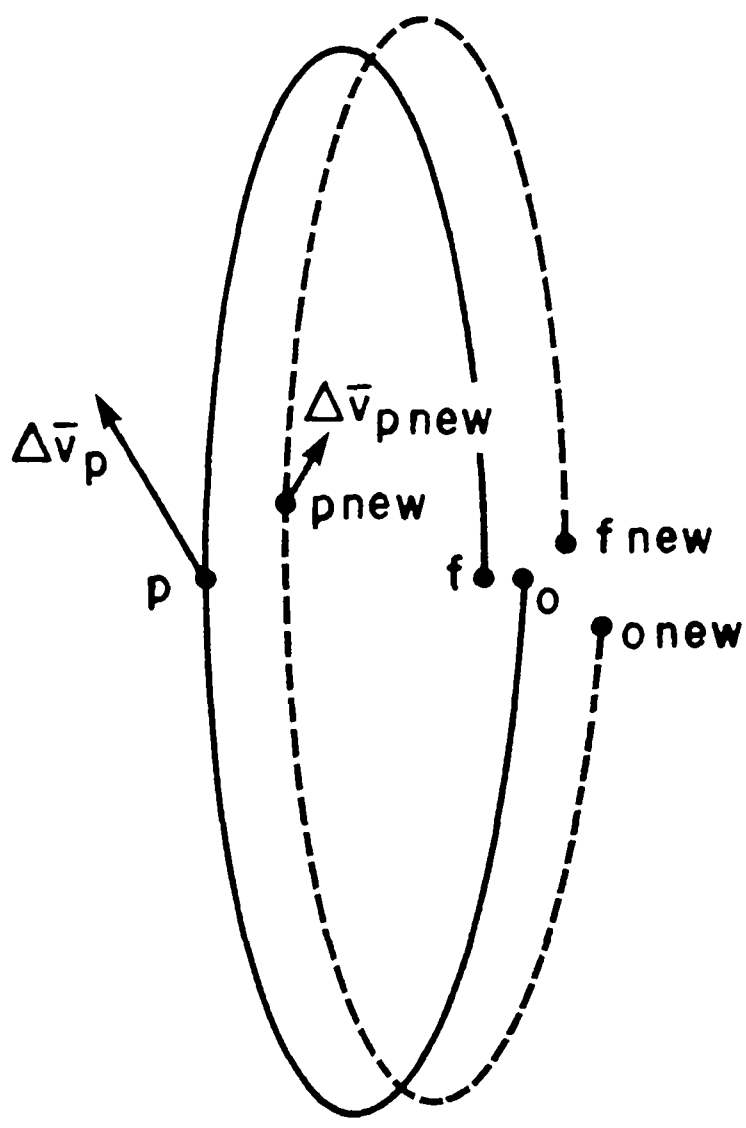

Fig. 2. One revolution trajectory: initial path and adjustment to reduce $\Delta\bar{v}$.

trajectory. Note that since a Lissajous trajectory does not repeat after a revolution, points '*o*' and '*f*' will not coincide.

The segments are then constructed in the following three steps: (i) A first guess is required for the state vector at *each* of the target points, and the analytic approximations can be used. There appears to be no advantage in using any approximation beyond third-order in this problem. As will be noted later lower-order expansions also provided suitable guesses in some cases. In regions far beyond the range of applicability of the analytic solution, a continuation method was successfully employed to obtain first guesses for the target point state vectors. In the example, the first guess for the initial point state vector is $X_0 = \{x_0, y_0, z_0, \dot{x}_0, \dot{y}_0, \dot{z}_0\}^T$, and vector states associated with the other target points are X_p and X_f. It t_j is defined as time of arrival at position 'j', the segment times $t_p - t_0$ and $t_f - t_p$ are also obtained. (ii) The first segment is computed by numerically integrating X_0, along with the transition matrix, for the time $t_p - t_0$ to the point 'p^*'. In general, the state values at 'p^*' will not equal the target values at 'p' since a Lissajous trajectory does not actually exist through all the states at 'o' and 'p'. It is temporarily assumed, however, that at least the positions x_0, y_0, z_0 and x_p, y_p, z_p are accurate. A differential corrections process is used to change the velocity at 'o' to meet the position requirement at 'p'. The vector relationship can be written

$$\delta X_{p^*} \cong \Phi(t_{p^*}, t_0)\delta X_0 + \frac{\partial X}{\partial t}\Bigg]_{p^*} \delta(t_{p^*} - t_0), \tag{7}$$

where $\partial X/\partial t$ is being evaluated at 'p^*'. The first three scalar equations contain four unknown: changes in the velocity components $\delta\dot{x}_0$, $\delta\dot{y}_0$, $\delta\dot{z}_0$ and change in the segment time $\delta(t_{p^*} - t_0)$. There are, of course, infinitely many solutions. However, the scalar equations can be rearranged into the linear form

$$L\bar{u} = \bar{b}, \tag{8}$$

where

$$L = \begin{bmatrix} \Phi_{14} & \Phi_{15} & \Phi_{16} & \dot{x} \\ \Phi_{24} & \Phi_{25} & \Phi_{26} & \dot{y} \\ \Phi_{34} & \Phi_{35} & \Phi_{36} & \dot{z} \end{bmatrix}_{p^*}$$

$$\bar{u} = \{\delta\dot{x}_0, \delta\dot{y}_0, \delta\dot{z}_0, \delta(t_{p^*} - t_0)\}^T$$

$$\bar{b} = \{\delta x_p, \delta y_p, \delta z_p\}^T,$$

and where Φ_{ij} is an element of $\Phi(t_{p^*}, t_0)$. The last three scalar equations in (7) are not used. Assuming that all the unknowns in $\bar{u}$ have equal importance, a result from linear algebra states that the solution to Equation (8) with the smallest Euclidean norm is given by

$$\bar{u} = L^T(LL^T)^{-1}\bar{b}. \tag{9}$$

The integration is restarted at t_0 with the new initial state 'o' and proceeds for the new time interval. The process is repeated until the position 'p^*' is equal to the position 'p' within some small tolerance. (Note that the velocities $\dot{x}_p$, $\dot{y}_p$, $\dot{z}_p$ are never used in computing segment one.) (iii) The second segment is computed in an identical manner, using X_p as the initial condition and X_f as the target. Assuming no change in x_p, y_p, z_p and t_p, the velocity components $\dot{x}_p$, $\dot{y}_p$, $\dot{z}_p$ and the arrival time t_f are adjusted to guarantee passage through the predetermined target position x_f, y_f, z_f.

The two segments are now patched together. In calculation of both segments, initial and endpoint positions are fixed, and the process corrects velocity so that the resulting path is continuous in position (within the tolerance used) as indicated by the solid line in Figure 2.

2.3.3. *$\Delta\bar{v}$ Reduction at the Maneuver Point*

In determining position continuity, no provision was made for velocity and, thus, a $\Delta\bar{v}$ will exist at point 'p'. So attention is now focused on reducing the $\Delta\bar{v}$. The procedure in general varies the positions of the target points to minimize the $\Delta\bar{v}$'s that will exist at each of these maneuver positions. The method has some similarities with one which has been used in determining interplanetary trajectories with multiple flybys [9].

Again examine the one revolution trajectory from 'o' to 'f'. If the change in $\Delta\bar{v}$ can be expressed as a function of the change in positions of 'o', 'p', 'f' and changes in the segment times, then these changes may be computed to drive the $\Delta\bar{v}$ to zero. Begin with the second segment and consider integration backwards from point 'f' to point 'p'. Let the symbol p^+ indicate conditions at 'p' on segment two and p^- the conditions at the same point but on segment one. The state X_{p^+} is a function of X_f and a relationship between them can be written in vector form as

$$\delta X_{p^+} \cong \Phi(t_p, t_f)\delta X_f + \dot{\frac{\partial X}{\partial t}}\bigg|_{p^+} \delta(t_{p^+} - t_f). \tag{10}$$

It is convenient to define the following three-dimensional vectors

$$\bar{r} = \{x, y, x\}^T$$

$$\bar{v} = \{\dot{x}, \dot{y}, \dot{z}\}^T$$

$$\bar{a} = \{\ddot{x}, \ddot{y}, \ddot{z}\}^T.$$

Also, divide the transition matrix into four submatrices, each 3×3, such that

$$\Phi(t_p, t_f) = \begin{bmatrix} A_{pf} & B_{pf} \\ C_{pf} & D_{pf} \end{bmatrix}.$$

Equation (10) can then be rewritten in the form

$$\begin{Bmatrix} \delta\bar{r}_{p^+} \\ \delta\bar{v}_{p^+} \end{Bmatrix} = \begin{bmatrix} A_{pf} & B_{pf} \\ C_{pf} & D_{pf} \end{bmatrix} \begin{Bmatrix} \delta\bar{r}_f \\ \delta\bar{v}_f \end{Bmatrix} + \begin{Bmatrix} \bar{v}_{p^+} \\ \bar{a}_{p^+} \end{Bmatrix} (\delta t_{p^+} - \delta t_f). \tag{11}$$

Solving the first vector equation for $\delta\bar{v}_f$

$$\delta\bar{v}_f = B_{pf}^{-1}\,\delta\bar{r}_{p^+} - B_{pf}^{-1}\,A_{pf}\,\delta\bar{r}_f - B_{pf}^{-1}\,\bar{v}_{p^+}(\delta t_{p^+} - \delta t_f). \tag{12}$$

Substitution of Equation (12) into the second vector equation of (11) yields

$$\begin{aligned}\delta v_{p^+} = {} & (C_{pf} - D_{pf}\,B_{pf}^{-1}\,A_{pf})\delta\bar{r}_f + D_{pf}\,B_{pf}^{-1}\,\delta\bar{r}_{p^+} - \\ & - (D_{pf}\,B_{pf}^{-1}\,\bar{v}_{p^+} - \bar{a}_{p^+})(\delta t_{p^+} - \delta t_f).\end{aligned} \tag{13}$$

A similar expression can be written for the trajectory segment from 'o' to 'p' as

$$\begin{aligned}\delta\bar{v}_{p^-} = {} & (C_{p0} - D_{p0}\,B_{p0}^{-1}\,A_{p0})\delta\bar{r}_0 + D_{p0}\,B_{p0}^{-1}\,\delta\bar{r}_{p^-} - \\ & - (D_{p0}\,B_{p0}^{-1}\,\bar{v}_{p^-} - \bar{a}_{p^-})(\delta t_{p^-} - \delta t_0).\end{aligned} \tag{14}$$

Subtracting Equation (14) from Equation (13) and constraining position and time at point 'p' to be the same for both segments, i.e. $\bar{r}_{p^+} = \bar{r}_{p^-}$ and $t_{p^+} = t_{p^-}$ produces

$$\delta\Delta\bar{v}_p = [M_0\,M_{t_0}\,M_p\,M_{t_p}\,M_f\,M_{t_f}]\begin{Bmatrix}\delta\bar{r}_0\\ \delta t_0\\ \delta\bar{r}_p\\ \delta t_p\\ \delta\bar{r}_f\\ \delta t_f\end{Bmatrix} \tag{15}$$

where the M matrices are defined as

$$M_0 = D_{p0}\,B_{p0}^{-1}\,A_{p0} - C_{p0}$$

$$M_{t_0} = \bar{a}_{p^-} - D_{p0}\,B_{p0}^{-1}\,\bar{v}_{p^-}$$

$$M_p = D_{pf}\,B_{pf}^{-1} - D_{p0}\,B_{p0}^{-1}$$

$$M_{t_p} = D_{p0}\,B_{p0}^{-1}\,\bar{v}_{p^-} - D_{pf}\,B_{pf}^{-1}\,\bar{v}_{p^+} + \bar{a}_{p^+} - \bar{a}_{p^-}$$

$$M_f = C_{pf} - D_{pf}\,B_{pf}^{-1}\,A_{pf}$$

$$M_{t_f} = D_{pf}\,B_{pf}^{-1}\,\bar{v}_{p^+} - \bar{a}_{p^+}.$$

Since it is desired to drive $\Delta\bar{v}_p$ to zero, $\delta\Delta\bar{v}_p = -\Delta\bar{v}_p$.

The vector equation in (15) contains three scalar equations and twelve unknowns. The system then has many solutions. But again, a conservative choice is that solution with the smallest norm which can be computed as previously discussed in Equations (8) and (9). The solution is essentially an updated guess for the state vectors at all the target points. The entire procedure is now repeated. With new target states, a continuous path is sought between the target positions by construction of the required segments. The updated trajectory for the example is represented by the dashed line in Figure 2. Once the new trajectory is computed, it will also have a $\Delta\bar{v}$ at point 'p'; however, because of the corrections made to the target positions, the $\Delta\bar{v}$ will be substantially smaller. The entire process may be repeated for as many iterations as necessary to bring the velocity discontinuity to

within some acceptable tolerance. The result is a Lissajous trajectory essentially continuous in position and velocity.

2.3.4. *Trajectory Determination for N_R Revolutions*

From a single trajectory, the method can be generalized for an arbitrary number of revolutions. Using the analytic approximation or a previous numerical result, target states and times are established at defined intervals (usually a half revolution) for N_R revolutions. The first target point is synonymous with the initial point and denoted as 'o'. Subsequent points are labelled as '1', '2',... 'n', so that n trajectory segments are defined. As in the single revolution case, the n target points plus point 'o' are used to construct trajectory segments which pass through the appropriate target positions with $\Delta\bar{v}$'s between each pair of segments. The changes in the target positions and times are then related to the $\Delta\bar{v}$'s in a generalized form of Equation (15) as

$$[M]\{\delta\bar{r}\} = \{-\Delta\bar{v}\}, \tag{16}$$

where

$$\{\delta\bar{r}\} = \begin{Bmatrix} \delta\bar{r}_0 \\ \delta t_0 \\ \delta\bar{r}_1 \\ \delta t_1 \\ \delta\bar{r}_2 \\ \delta t_2 \\ \delta\bar{r}_3 \\ \delta t_3 \\ \vdots \\ \delta\bar{r}_n \\ \delta t_n \end{Bmatrix}, \qquad \{-\Delta\bar{v}\} = \begin{Bmatrix} -\Delta\bar{v}_1 \\ -\Delta\bar{v}_2 \\ -\Delta\bar{v}_3 \\ \vdots \\ -\Delta\bar{v}_{n-1} \end{Bmatrix}$$

and

$$[M] = \begin{bmatrix} M_{0_1} & M_{t_{0_1}} & M_{p_1} & M_{t_{p_1}} & M_{f_1} & M_{t_{f_1}} & 0 & 0 & 0 & 0 & \dots & 0 \\ 0 & 0 & M_{0_2} & M_{t_{0_2}} & M_{p_2} & M_{t_{p_2}} & M_{f_2} & M_{t_{f_2}} & 0 & 0 & \dots & 0 \\ 0 & 0 & 0 & 0 & M_{0_3} & M_{t_{0_3}} & M_{p_3} & M_{t_{p_3}} & M_{f_3} & M_{t_{f_3}} & \dots & 0 \\ & \cdot & & & & & \cdot & & \cdot & & & \\ & & \cdot & & & & & \cdot & & \cdot & & \\ & & & \cdot & & & & & \cdot & & \cdot & \\ 0 & 0 & 0 & 0 & \dots & & M_{0_{n-1}} & M_{t_{0_{n-1}}} & M_{p_{n-1}} & M_{t_{p_{n-1}}} & M_{f_{n-1}} & M_{t_{f_{n-1}}} \end{bmatrix}$$

M is of dimension $(3n-3) \times (4n+4)$, $\delta\bar{r}$ is a column vector of length $(4n+4)$ and $\Delta\bar{v}$ a column vector with $(3n-3)$ elements for $n \geqslant 2$. The solution which minimizes

$||\delta\bar{r}||$ is

$$\delta\bar{r} = -M^T(MM^T)^{-1}\Delta\bar{v} \tag{17}$$

With these new positions and times, the process is repeated, and the $\Delta\bar{v}$'s will again be simultaneously reduced. In the numerous cases examined, five iterations were usually sufficient to bring all the $\Delta\bar{v}$'s to an acceptably small magnitude.

3. Results

A large number of Lissajous trajectories have been determined to date. The procedure was coded and run on a Cyber 205 computing machine at Purdue University. Representative trajectories have been calculated which are associated with libration points at both L_1 and L_2; in both the Sun–Earth and Earth–Moon systems; at a wide range of in-plane and out-of-plane amplitude combinations; and in regions where the approximate analytic solution breaks down. Some examples are discussed below.

CASE 1: SMALL TRAJECTORY ABOUT L_1 IN THE SUN–EARTH/MOON BARYCENTER SYSTEM

The three planar projections of this path, calculated in the Sun–Earth/Moon barycenter system, are shown in Figure 3. Recall that the origin is located at L_1. It is computed for 5 revolutions, or approximately 2.4 years, although any length could have been chosen. The initial point on the trajectory is at the maximum value of z in the x–z plane. Some of the numerical details are presented in Table I.

TABLE I

Small trajectory about L_1 in the Sun–Earth/Moon barycenter system ($\mu = 3.04 \times 10^{-6}$)

Initial conditions

Analytic (3rd Order): $\phi = 180°$ $A_y = 300\,000$ km; $\psi = 90°$ $A_z = 150\,000$ km

5 Revolution Trajectory (10 Segments)

Target Point ($\bar{r}_i$) i	Initial Velocity Discontinuity (m/s) $\lvert\Delta\bar{v}\rvert_i$	Position Difference (km) $\lvert\bar{r}_i^N - \bar{r}_i^A\rvert$	Velocity Difference (m/s) $\lvert\bar{v}_i^N - \bar{v}_i^A\rvert$
0	—	697.89	0.82
1	3.67	862.83	0.46
2	3.85	697.38	0.39
3	3.33	432.23	0.45
4	3.40	463.12	0.41
5	2.73	196.48	0.44
6	2.73	566.97	0.44
7	2.01	325.24	0.46
8	1.99	703.43	0.49
9	1.34	507.45	0.47
10	—	397.12	0.59

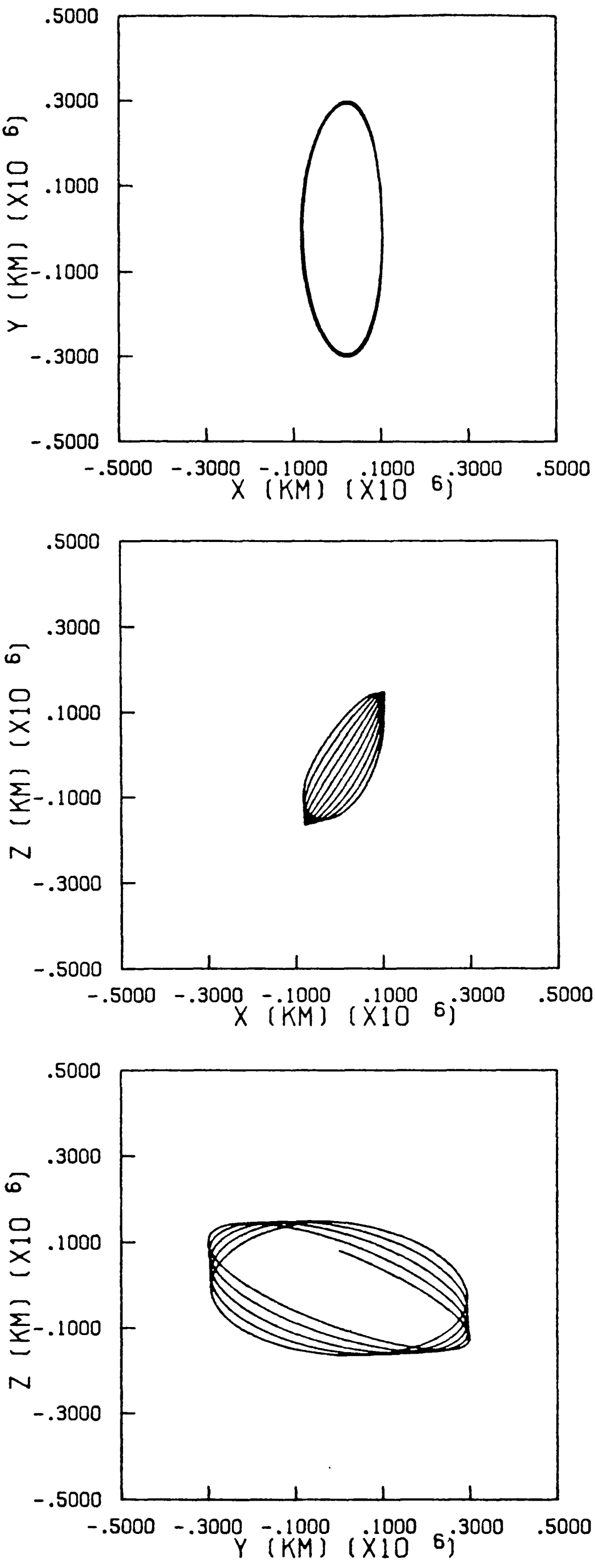

Fig. 3. Small L_1 trajectory ($A_y = 300\,000$ km, $A_z = 150\,000$ km).

The input indicates that the initial guess is obtained from a third-order analytic solution and that an orbit is sought with an in-plane y amplitude of approximately 300 000 km and an out-of plane z amplitude of approximately 150 000 km. The target points are identified at $\bar{r}_0$ and approximately at each subsequent half revolution. From an initial guess for the state (position and velocity) at each target point, a continuous path through those positions is found that contains velocity discontinuities (or required maneuvers) of magnitude $|\Delta\bar{v}|$ at each $\bar{r}_i$, shown in the second column of the table. The $\Delta\bar{v}$'s are iteratively reduced until each $|\Delta\bar{v}| < 1 \times 10^{-7}$ m/s, considered here to be zero. Actually, all the values in this case are less than 0.01 m/s after one iteration. Thus, the total $|\Delta\bar{v}|$ for the entire trajectory, 25.06 m/s, was successfully reduced to 'zero' for the 5 revolutions considered. The result is the path plotted in Figure 3. This trajectory is small and the analytic solution (A) could be expected to produce a good approximation. On the scale shown in the figure, the differences in the initial ($\bar{r}^A$) and final, numerically determined ($\bar{r}^N$), target positions are not obvious. However, a comparison of the values shows that the locations still differ by hundreds of kilometers, over 850 km at one point. The velocity differences are all less than 1 m/s. Recall that the time is also varied in the reduction process. The resulting differences in the times at each target only changed on the order of a few seconds. If total trajectory time is constrained, a solution is still obtained with small differences in segment times and states.

CASE 2: LARGE TRAJECTORY ABOUT L_1

Shown in Figure 4 is a 5 revolution Lissajous path which is much larger than that contained in the previous case at the same value of μ. The input in Table II indicates that the initial guess is again obtained from an analytic third-order solution. The reference amplitudes are $A_y = 700\,000$ km and $A_z = 900\,000$ km, considered to be large. For the numerical solution, the target points are identified at quarter revolutions, dividing the trajectory into 20 segments. The analytic solution is not expected to be a good approximation at this orbit size, and the results in Table II confirm that view. Because the approximation is poor, the larger number of segments was required to assure convergence of the inner level iterations. The magnitudes of the velocity discontinuities average 46 m/s, also because of a poor initial guess for the states. After two iterations the $\Delta\bar{v}$'s are all cut to less than 1 m/s. When all the $\Delta\bar{v}$'s have been driven to zero, the position variations of the targets is significant. As may be seen in the table, many positions are adjusted by more than 100 000 km. The times to reach these new $\bar{r}_i$ are adjusted only on the order of minutes. The resulting path is plotted as the solid line in Figure 4. Note that the primary μ is located approximately 1.5×10^6 km from L_1 on the positive x-axis. The first obvious fact in the figure is that the maximum y and z distances from L_1 vary significantly from one revolution to the next to a much greater extent than in the smaller orbit in Case 1. The A_y value of 700 000 km is closer to an 'average' maximum value of y. Also plotted in Figure 4 are points calculated directly from the

TABLE II
Large trajectory about L_1 ($\mu = 3.04 \times 10^{-6}$)

Initial Conditions

Analytic (3rd) Order:	$\phi = 180°$	$A_y = 700\,000$ km
	$\psi = 90°$	$A_z = 900\,000$ km

5 Revolution Trajectory (20 segments)

Target Point ($\bar{r}_i$) i	Initial Velocity Discontinuity (m/s) $\lvert\Delta\bar{v}\rvert_i$	Position Difference (km) $\lvert\bar{r}_i^N - \bar{r}_i^A\rvert$	Velocity Difference (m/s) $\lvert\bar{v}_i^N - \bar{v}_i^A\rvert$
0	—	178677	115.1
1	57.2	250317	60.4
2	74.2	104366	90.3
3	23.1	252027	34.7
4	90.9	79033	115.4
5	64.5	157663	46.0
6	50.5	77400	63.3
7	26.1	115331	44.4
8	47.3	38532	79.0
9	72.0	95207	54.9
10	46.0	120616	47.0
11	27.1	70658	54.9
12	32.5	51589	45.4
13	59.3	88985	54.8
14	36.3	133187	50.2
15	31.4	96482	56.7
16	30.6	94539	23.3
17	47.5	112061	41.3
18	19.3	113095	64.2
19	38.9	132975	50.0
20	—	65217	57.3

anlaytic expression. The inaccurate approximation was, however, used successfully in this case for a numeric solution.

Some observations are apparent from this and other large trajectories that have been determined. There are an infinite number and variety of Lissajous trajectories. As size increases, the nearly periodic nature seen in the x–y planar views of smaller orbits is degraded as the nonlinear effects become increasingly significant at larger amplitudes, as seen in Figure 4. The degradation might be less severe in a different trajectory. Interestingly, such a case was located utilizing a different initial guess, i.e. the second-order analytic result, and is plotted in Figure 5. This solution is also obtained by using 20 segments. The initial values of $|\Delta\bar{v}|$ averaged 32.5 m/s, lower than the third-order guess. The second-order expression did predict a slightly smaller orbit size, perhaps contributing to the tighter integrated result. The smaller $\Delta\bar{v}$'s are somewhat misleading however. In reducing the $\Delta\bar{v}$'s to zero to obtain the path in Figure 5, the positions shift by larger amounts – almost half the target points

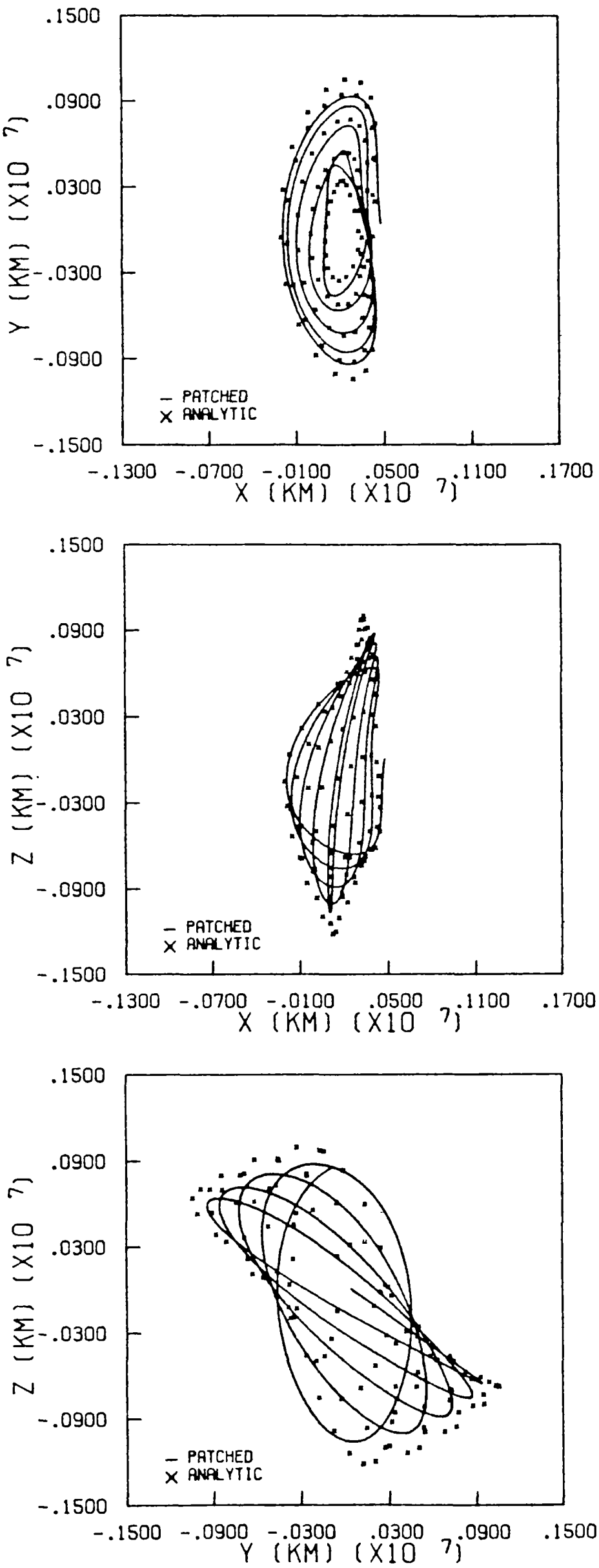

Fig. 4. Large L_1 trajectory computed from a third-order initial guess ($A_y = 700\,000$ km, $A_z = 900\,000$ km).

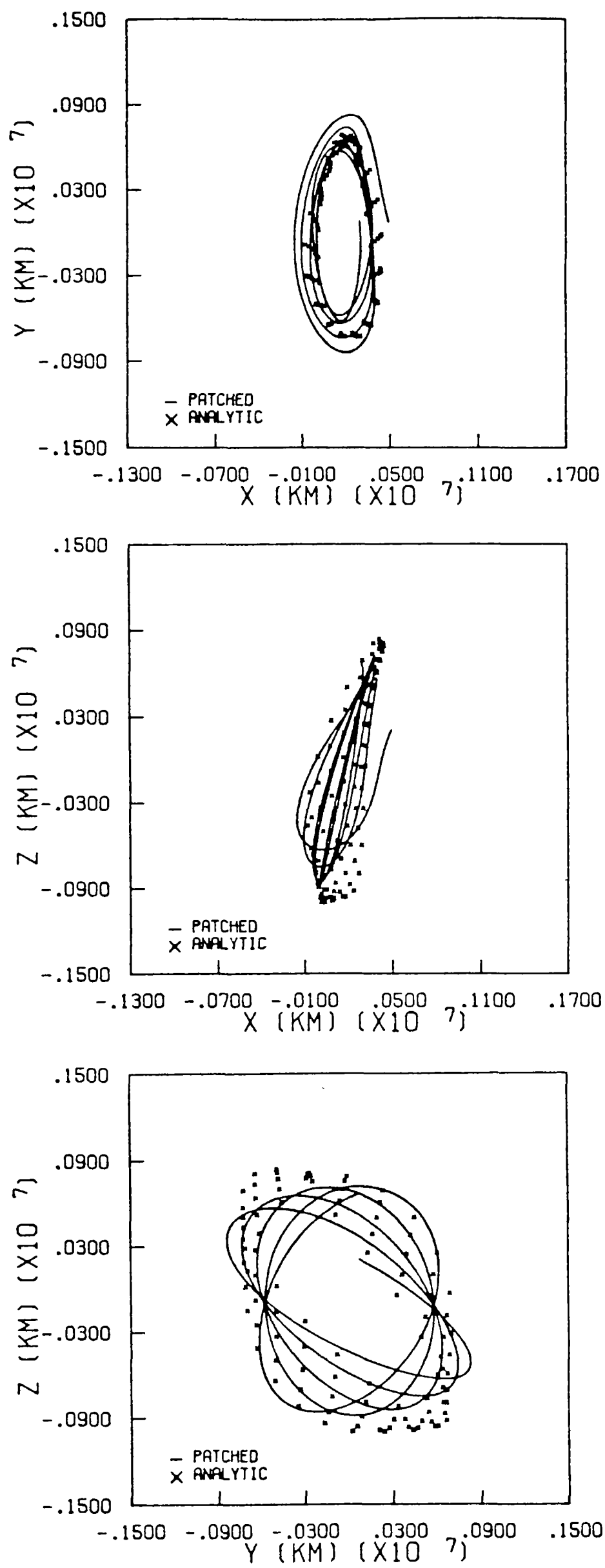

Fig. 5. Large L_1 trajectory computed from a second-order initial guess ($A_y = 700\,000$ km, $A_z = 900\,000$ km).

are adjusted by 200 000 km or more. It is also of interest that the total trajectory time in Figure 5 is approximately 8 days less than the solution in Figure 4. In both of these solutions, it is apparent in the figures that the trajectory endpoints are not constrained. That possibility is expected to be pursued.

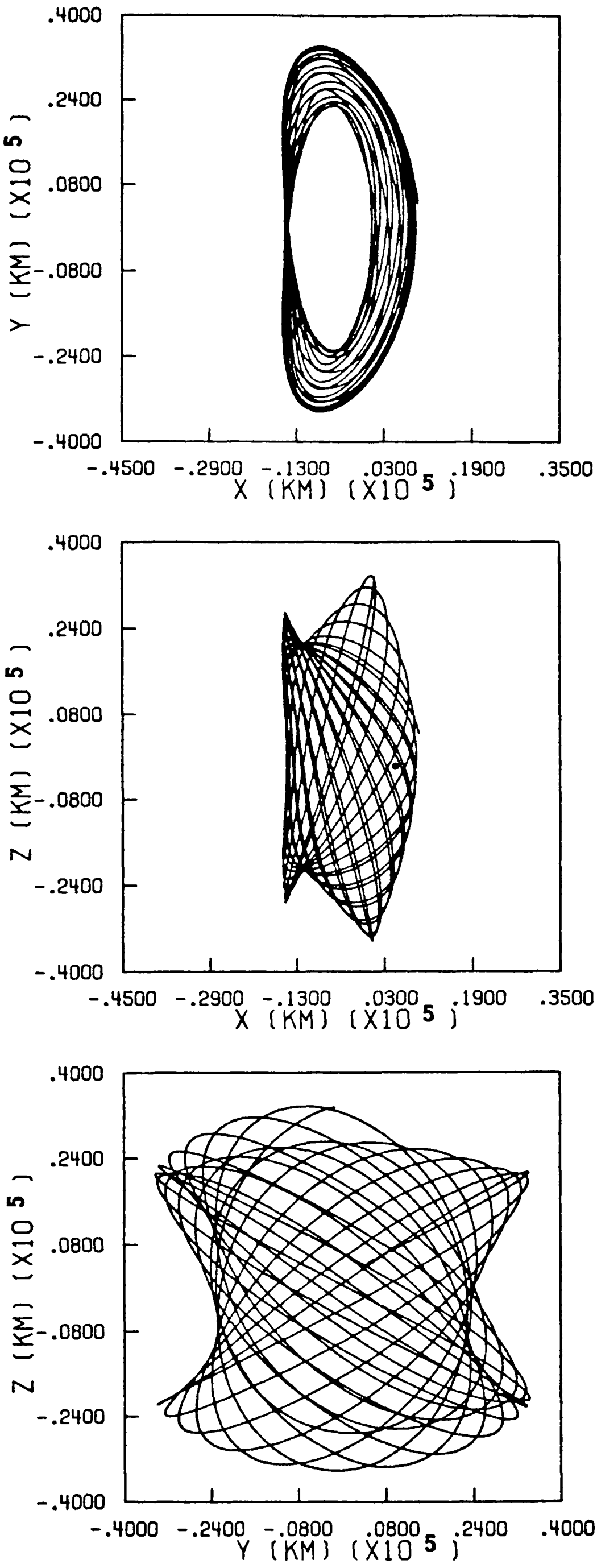

Fig. 6. L_2 trajectory in the Earth–Moon system ($A_y = A_z = 30\,000$ km).

Any Lissajous trajectory determined numerically is more predictable, of course, by using better initial guesses. A continuation method could be employed to update target positions and velocities from a previous solution. It does afford some identification and selection of characteristics, such as maximum and minimum amplitudes over a given number of revolutions. Large orbits have been successfully produced with such a procedure. Using a reasonable step beyond a previous solution, a new solution is found, frequently requiring only half the number of segments that is needed in the example above, and not surprisingly, the initial $\Delta\bar{v}$'s may be smaller. Solutions are also continued into regions where the analytic approximation has totally lost its usefulness. A major disadvantage, of course, of an approach which steps along solutions is that a large number of trajectories must be determined before the desired orbit size is achieved.

CASE 3: TRAJECTORY ABOUT L_2 IN THE EARTH–MOON SYSTEM

The final example is a large trajectory associated with a different collinear point, L_2, in the Earth–Moon system. To vary N_R, this trajectory is calculated for 18 revolutions, or about 264 days. The resulting 72 integrated segments are shown in Figure 6, where the origin is now L_2. Table III contains numerical information for some of the target points. The orbit size is represented by the input amplitudes $A_y = A_z = 30\,000$ km. This is the only example shown in which the input seeks a trajectory with approximately equal in-plane and out-of-plane amplitudes although numerous other such cases have been run. The Moon is located approximately 65 000 km from L_2 in the $-\hat{\mathrm{x}}$ direction. The initial states are approximated from the third-order analytic expression. All of the $\Delta\bar{v}$'s are reduced simultaneously and are below 1 m/s after two iterations, but a total of ten iterations is required to reduce all 71 magnitudes below 10^{-7} m/s. In that reduction process, the target positions are shifted by thousands of kilometers which is quite a significant amount for an orbit of 30 000 km amplitude. The time associated with each segment is adjusted up to 36 minutes, as well, and includes both increases and decreases.

The larger value of μ in this system did not cause any particular difficulties in obtaining a solution, nor did the increased number of revolutions. Large values of N_R have been used with the smaller μ value as well.

4. Concluding Remarks

Numerical determination of Lissajous trajectories is accomplished with an iterative scheme which reduces position and velocity discontinuities to zero. The examples shown here were computed for two specific values of μ, however, the approach is quite general and will apply in a wide range of primary systems. It is intended to extend the calculation of these trajectories to the elliptic restricted problem and include additional perturbations.

TABLE III

Large trajectory about L_2 in the earth–moon system ($\mu = 0.012$)

Initial Conditions		
Analytic (3rd order):	$\phi = 180°$	$A_y = 30\,000$ km
	$\psi = 90°$	$A_z = 30\,000$ km

18 Revolution Trajectory (72 segments)

Target Point ($\bar{r}_i$) i	Initial Velocity Discontinuity (m/s) $\lvert\Delta\bar{v}\rvert_i$	Position Difference (km) $\lvert\bar{r}_i^N - r_i^A\rvert$	Velocity Difference (m/s) $\lvert\bar{v}_i^N - \bar{v}_i^A\rvert$
0	—	5716	21.0
8	16.1	3547	22.1
16	8.9	3173	25.6
24	2.1	2311	25.5
32	9.2	4609	18.3
40	15.7	5198	10.7
48	21.5	5304	6.3
56	16.1	7727	1.4
64	8.9	8101	16.8
72	—	6397	31.8

Acknowledgments

Portions of this work have been supported by the National Science Foundation under Grant No. MSM-8352281, and by Computer Sciences Corporation under Contract No. 012607C01. The authors are grateful to CSC for making some of the analytic software available.

References

1. Farquhar, R. W. and Kamel, A. A.: 1973, 'Quasi-Periodic Orbits About the Translunar Libration Point,' *Celes. Mech.* **7**, 458.
2. Richardson, D. L. and Cary, N. D.: 1975, 'A Uniformly Valid Solution for Motion About the Interior Libration Point of the Perturbed Elliptic-Restricted Problem,' *AAS Paper*, 75–021.
3. Davoust, E.: 1986. 'Periodic Orbits in Elliptical Galaxies II. Rotation about the Axis of Symmetry,' *Astron. & Astrophys.*, **156**, 152.
4. Richardson, D. L.: 1978, 'Periodic Orbits About the L_1 and L_2 Collinear Points in the Circular-Restricted Problem,' Computer Sciences Corporation Report CSC/TR–78/6002.
5. Breakwell, J. V. and Brown, J. V.: 1979, 'The 'Halo' Family of 3-Dimensional Periodic Orbits in the Earth–Moon Restricted 3-Body Problem,' *Celes. Mech.* **20**, 389.
6. Zagouras, C. G. and Kazantzis, P. G.: 1979, 'Three Dimensional Periodic Oscillations Generating from Plane Periodic Ones Around the Collinear Lagrangian Points,' *Astrophys. Space Sci.* **61**, 389.
7. Richardson, D. L.: 1980, 'Halo Orbit Formulation for the ISEE-3 Mission,' *J. Guidance and Control* **3**, 543.
8. Howell, K. C.: 1984, 'Three-Dimensional, Periodic, 'Halo' Orbits,' *Celes. Mech.* **32**, 53.
9. D'Amario, L. A., Byrnes, D. V., Sackett, L. L., and Stanford, R. H.: 1979, 'Optimization of Multiple Flyby Trajectories,' *ASS Paper*, 79–162.